The effect of oxygen-to-argon ratio on the electrical and reliability characteristics of sputtered $Sr_{0.8}Bi_{2.5}Ta_{1.2}Nb_{0.9}O_{9+x}$ thin films

M.S. Tsai, T.Y. Tseng*

Department of Electronics Engineering and Institute of Electronics, National Chiao Tung University, Hsinchu 30050, Taiwan

Abstract

This work investigated how the annealing process affects the ferroelectric properties of thin films of $Sr_{0.8}Bi_{2.5}Ta_{1.2}Nb_{0.9}O_{9+x}$ (SBTN) on $Ir/SiO_2/Si$ substrates prepared by two-target off-axis rf magnetron sputtering at various $O_2/(Ar + O_2)$ mixing ratios (OMR) with a substrate temperature of 570°C. Experimental results indicated that the annealing could effectively result in a large remanent polarization. The remanent polarization, dielectric constant and leakage current of 598°C post-annealing SBTN thin films increased with an increase in the OMR and reached a maximum value at 40% OMR. In addition, the results obtained from the dielectric constant and the leakage current were interpreted in terms of polarization effect and loss theory. The 400-nm thick 40% OMR SBTN films with 598°C post-annealing exhibited good surface morphology and had a dielectric constant of 752, a loss tangent of 0.035 at 100 kHz, a leakage current density of 6×10^{-6} A/cm^2 at an electric field of 50 kV/cm with a delay time of 30 s, a remanent polarization ($2P_r$) of 40 $\mu C/cm^2$, a coercive field ($2E_c$) of 77 kV/cm at an applied voltage of 3 V, and a measured value of Q_{sw} of 20 $\mu C/cm^2$. According to studies on the 10-year lifetime of time-dependent dielectric breakdown (TDDB), high OMR samples have a longer lifetime than the other lower OMR samples. The SBTN films demonstrated fatigue free characteristics up to 10^{11} switching cycles under a 3-V bipolar 1 MHz square wave. Moreover, the polarization of the films decreases slightly (less 0.5% per decade) with retention time up to 240 min. © 2000 Elsevier Science S.A. All rights reserved.

Keywords: Sputtering; SBT; Reliability; Ferroelectric properties

1. Introduction

Ferroelectric materials have remanent polarization with two distinct states which an applied electric field can reverse. These materials have the potential for non-volatile random access memory applications (NVRAM) [1−4]. Ferroelectric memories offer several advantages over silicon-based memories, such as faster write speeds and lower operating voltages. As is increasingly being recognized, ferroelectric thin films, such as lead zirconate titanate (PZT), are highly promising for non-volatile memory applications, e.g.

ferroelectric RAM devices (FRAM) [5,6]. These ferroelectric films exhibit properties capable of satisfying the basic materials requirement for low power memory applications; these properties have a high remanent polarization, low coercive fields, and high resistance. However, PZT materials for FRAM device applications and fabrications still have several problems, such as fatigue, aging, retention, and imprint. Among them, fatigue, i.e. a decrease in switchable polarization with an increasing number of polarization reversals, is a pertinent reliability issue for FRAM devices using a destructive readout operation (switching of polarization at each read/write operation). Applying oxide electrodes is an effective means of improving the fatigue characteristics of PZT-based capacitors [7]. Although

* Corresponding author. Tel.: +886-572-1879; fax: +886-573-4361.
  E-mail address: tseng@cc.nctu.edu.tw (T.Y. Tseng).

the above techniques have improved the fatigue rate of PZT-based thin films, the electrical conductivity of oxide electrodes is not as high as those of the metal electrodes normally used, such as Pt. Lower conductivity of the oxide electrodes can induce undesirable characteristics of ferroelectric NVRAM, such as a higher RC time constant of the capacitor. In addition, oxide electrodes may lead to the formation of secondary non-ferroelectric phases during film growth if processing conditions are not carefully controlled [8].

Recent investigations have examined the feasibility of alternative materials, such as bismuth-layered oxides having a perovskite-like layer-type structure, for FRAM applications [9–13]. These investigations have identified thin films of bismuth-layered oxides, e.g. $SrBi_2Ta_2O_9$ (SBT) as fatigue-free materials displaying nearly no change (less than 5%) in remanent polarization up to 10^{12} switching cycles with Pt electrodes. Owing to the characteristics of resistance to fatigue, these layered bismuth oxides are considered to be the optimum material for NVRAM applications. Although considered highly promising for NVRAM applications, SBT thin films have not been completely characterized.

Commercialization of non-volatile FRAM technology based on SBT has been hampered by problems related to a high processing temperature ($> 750°C$), low remanent polarization ($2P_r$), and low Curie temperature (T_c), thereby making direct integration into high density CMOS devices extremely difficult [14]. In general, the difficulty in reducing the post-deposition annealing temperature of SBT thin films was largely attributed to poor ferroelectric properties at an annealing temperature lower than 700°C. Recent investigations indicated that $Sr_{0.8}Bi_{2.5}Ta_{1.2}Nb_{0.9}O_{9+x}$ (SBTN) can reduce the processing temperature ($\sim 600°C$) and improve the ferroelectric properties, as well as achieve a higher P_r and higher T_c than SBT [7,14–17]. Therefore, SBTN is a highly promising material for memory applications. Moreover, related investigations have confirmed the important role which oxygen vacancies play in the fatigue and reliability properties of ferroelectric films [6,7]. However, a systematic study of the effect of $O_2/(Ar + O_2)$ mixing ratio (OMR) during rf sputtering on the dielectric and electrical properties of SBTN thin films is generally lacking. In this work, we investigated the structural, electrical and dielectric properties of SBTN films on $Ir/SiO_2/Si$ substrates at a low temperature of 570°C prepared by two-target off-axis rf sputtering at various OMR.

2. Experimental

SBTN thin films were deposited on an $Ir/SiO_2/(100)Si$ bottom storage node electrode by two-target off-axis rf magnetron sputtering. The starting *p*-type silicon wafer was cleaned by the standard RCA cleaning process and then chemically etched in a dilute HF solution. The 100-nm thick SiO_2 layer was thermally grown at 1050°C in a dry oxidation furnace. The 100-nm thick Ir bottom electrode on the SiO_2/Si substrate was deposited using a separate sputtering system. Next, the Ir film was prepared at a fixed power of 50 W (the power density was 2.55 W/cm^2), a constant pressure of 5 mtorr and substrate temperature of 350°C. The measured resistivity of Ir was approximately 27 $\mu\Omega/cm$ at room temperature.

The SBTN films were deposited on Ir by simultaneous magnetron sputtering from two different sintered targets of $Sr_{0.8}Bi_{2.2}Ta_{1.2}Nb_{0.8}O_9$ and Bi_2O_3 with a diameter of 2 inches and a thickness of 1/8 inch, synthesized using the standard solid-state reaction process. The Bi_2O_3 target was used to compensate for Bi atoms in the deposited film because the Bi content in the film generally deviates strikingly from that of the target at a high substrate temperature. The sputtering chamber was then evacuated to a base pressure of 10 mtorr. All films were prepared at a fixed power of 100 W for the $Sr_{0.8}Bi_{2.2}Ta_{1.2}Nb_{0.8}O_9$ target (the power density was 5.10 W/cm^2) and 20 W for Bi_2O_3 target (power density is 1.01 W/cm^2). A constant chamber pressure of 20 mtorr was maintained by a mixture of argon and oxygen at various mixing ratios ranging from 1:1 to 1:0 with a total flow of 2 sccm. The target-to-substrate separation was approximately 5 cm. All of the SBTN films deposited at 570°C had the same thickness of approximately 400 nm. The deposition rate was approximately 24–35 Å/min at 570°C, as depicted in Fig. 1. According to this figure, the deposition rate decreased with increasing OMR, which was attributed to a decrease of the Ar flow. The 50-nm thick Pt top electrodes with diameters of 165, 255 and 350 μm, respectively, were then formed by dual E-Gun deposition and patterned by the shadow mask process. Finally, to understand the effect of post-annealing, part of the SBTN thin films after deposition (with Pt top electrode) were annealed at temperatures ranging from 598 to 673°C in a vacuum with pressure of 10 mtorr for 30 min.

The film thickness was determined from ellipsometry. The thickness measurement was further verified by examining the cross section of the film via scanning electron microscopy. The structure was characterized by X-ray diffraction (XRD; Siemens D5000). Based on XRD data, the average grain size could be determined by Scherrer's formula [18]. The chemical composition was estimated by inductively coupled plasma atomic emission spectrometry (ICP-AES; Perkin-Elmer SCIEX ELAN 5000, USA). The surface roughness and morphology were examined by atomic force microscopy (AFM; Digital Instruments Nano-Scope III). Next, the depth profiles of oxygen near the interface of SBTN/bottom electrodes were analyzed by secondary ion mass spectrometry (SIMS, CAMECA IMS-4f,
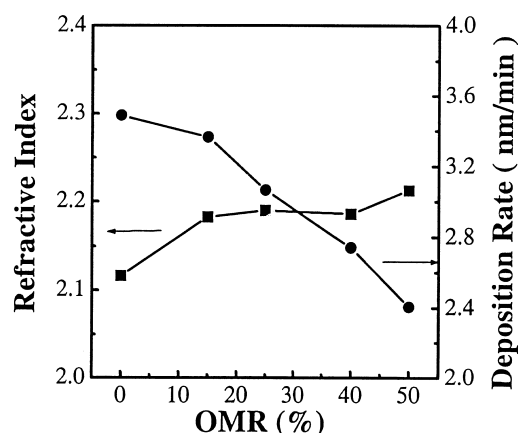
Fig. 1. The change in refractive index and deposition rate of SBTN thin films with various OMR.

France). The capacitance−voltage (C−V) characteristics were measured on the metal−insulator−metal (MIM) structure by measuring the capacitance at 100 kHz as a function of a swept positive-to-negative voltage bias. The dielectric constants of the films were then calculated from the capacitance measured at 100 kHz without bias voltage. The dielectric properties were measured as a function of frequency with a Hewlett−Packard (HP) 4194A impedance-gain phase analyzer. The current−voltage (I−V) was measured by measuring the current through the sample using HP4145B. A Pt top electrode of the SBTN capacitor was connected to the voltage source and the bottom electrode was grounded. Notably, the polarity was positive when a positive voltage was applied to the top electrode. The ferroelectric properties (fatigue, retention and polarization-electric field) of the films were measured using RT66A ferroelectric tester from Radiant Technologies. All data reported herein are the average values of ten specimens.

3. Results and discussion

Fig. 1 depicts the change in refractive index of SBTN thin films deposited at 570°C at various OMR. According to this figure, the refractive index of SBTN thin films increases with increasing OMR. Fig. 2a displays the XRD patterns of 400-nm thick SBTN thin films deposited at 570°C at 0, 25, 40 and 50% OMR. The film deposited at 0% OMR revealed that diffraction peaks appeared only from the Ir film and (008), (115), (028) and (220) peaks of perovskite SBTN structure, implying the absence of (200) and (0010) peaks. Although films deposited at 25 and 40% OMR contained the (200) peak of the perovskite SBTN structure, this peak had a low intensity. In addition, the (200) and (0010) peak intensities of the SBTN films increased with an increase in OMR. Comparing stronger and sharper perovskite peaks of (200) and (0010) from the

50% OMR films with those from the films deposited at a lower OMR revealed an improved crystallinity at high OMR films. This increased crystallinity may have contributed to the enhancement in the index of refraction with increasing OMR, as illustrated in Fig. 1. Fig. 2b displays the XRD patterns of 40% OMR films at 598°C and 673°C post-annealing. According to this figure, the (200) and (115) peaks of the 598°C post-annealing film were stronger and sharper than those of the 673°C post-annealing and as-deposited films. Hence, 598°C post-annealing can enhance the grain growth of the SBTN thin films in the a-axis and c-axis directions, and improve the crystallinity of the film. The variation of reflections from the (008) and (0010) planes present in the XRD pattern of SBTN (Fig. 2b) could be attributed to the change of the (111) texture in the underlying Ir bottom electrode during annealing. On the basis of the results shown in Fig. 2, the peaks from (00l) planes were small. It is known that SBT thin films exhibit a large polarization along the a- or b-axis; therefore, the orientation indicated in Fig. 2 was preferable to obtain large polarization.

Fig. 3 illustrates the atomic composition of various OMR SBTN thin films with 598°C, 640°C, and 673°C post-annealing. This composition, determined from
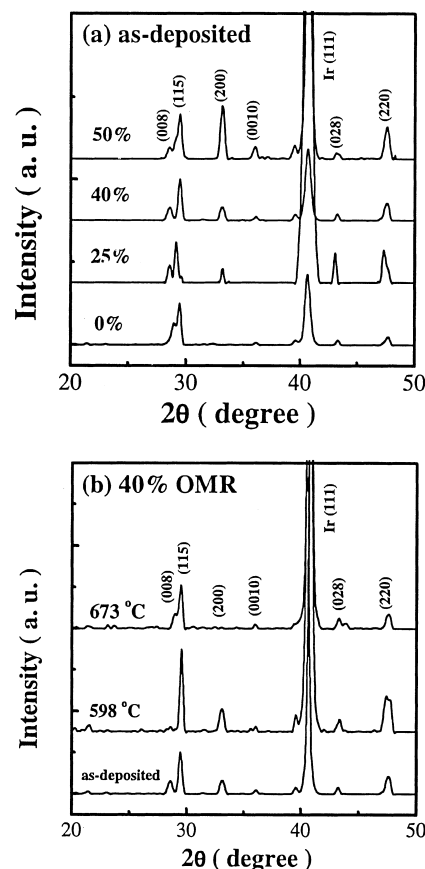

Fig. 2. XRD patterns of SBTN thin films with: (a) various OMR indicated; and (b) 40% OMR films with post-annealing.

ICP-AES, was represented by the atomic ratios of Bi, Sr, and Nb to Ta (= 1.2). An average atomic ratio of Sr/Nb/Ta was approximately 0.8:0.9:1.2, and almost no change occurred for the films obtained at various OMR and post-annealing. The average atomic ratios of Bi ranged from 2.3 to 2.7 within an error of 8%, which decreased with increasing OMR and annealing temperature. The composition of the 40% OMR film was substantially equal to $Sr_{0.8}Bi_{2.5}Ta_{1.2}Nb_{0.9}O_{9+x}$. In addition, the atomic concentrations of Bi decreased with an increase in OMR, which was attributed to the reduced sputtering rate of Bi atom (the atomic mass of Bi is heavier) at a higher OMR. In addition, the atomic concentration of Bi decreased with an increase in annealing temperature, which was attributed to the evaporation of Bi out of the films at a high annealing temperature.

The Bi content in the film varied with OMR and the annealing temperature was also analyzed using SIMS to confirm the atomic concentrations mentioned above. Closely examining the SIMS data in Fig. 4a–c revealed that the Bi concentration of the 25, 40, and 50% OMR films with 598°C post-annealing decreased with increasing OMR. In addition, the Bi concentration of 25% OMR films with 598°C and 673°C post-annealing de-
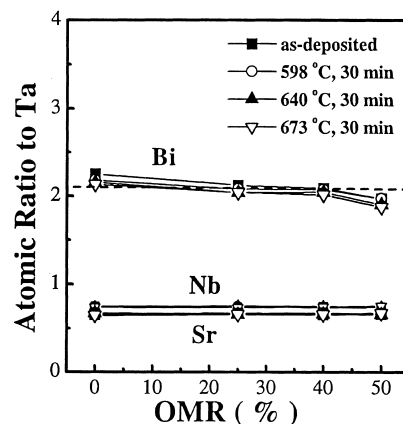

Fig. 3. The Bi, Nb, and Sr to Ta atomic ratios of SBTN films as a function of OMR and post-annealing temperature.

creased with an increase in annealing temperature, as illustrated in Fig. 4a,d. These results correlated well with those in Fig. 3. The Bi depth profiles of SBTN films (Fig. 4a,d) indicated that the interdiffusion of the constituent ions most likely accounted for the formation of a thin interfacial layer between the film and Ir electrode. Notably, the oxygen concentration at the interface of SBTN/Ir slightly increased with an
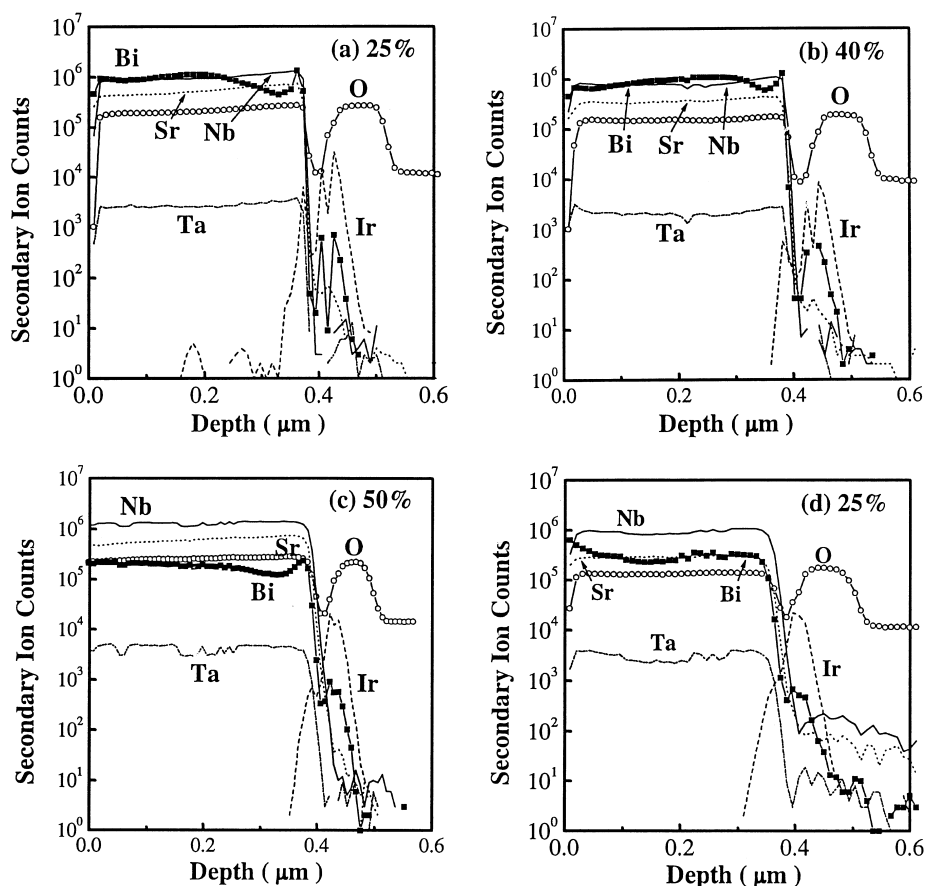

Fig. 4. SIMS depth profiles of SBTN films deposited at: (a) 25%; (b) 40%; (c) 50% OMR, with 598°C post-annealing; and (d) 25% OMR with 673°C post-annealing.

increase in OMR (Fig. 4a–c) because the Ir bottom electrode could be oxidized during the SBTN sputtering process.

Fig. 5a confirms that increasing the OMR during sputtering decreased the root mean square (r.m.s.) surface roughness of SBTN films, with and without post-annealing. Moreover, this decreased roughening of the films was attributed to the small grain size at high OMR (Fig. 5b). Fig. 5b indicates that the average grain size of the as-deposited SBTN thin films, determined by Scherrer's formula, decreased with an increase in OMR. The average grain size of 0% OMR films had a maximum value of 26 nm, while that of 50% OMR films had the smallest value of approximately 10 nm. It has been previously shown that the grain size of the barium strontium titanate calculated from the Scherrer's formula agrees with that determined by transmission electron microscopy (TEM) images [19]. Therefore, a TEM study was required to verify the grain size of the SBTN film. The r.m.s. surface roughnesses were 13.6, 9.7, 9.1 and 8.3 nm for 0, 25, 40 and 50% OMR films without post-annealing, respectively. In addition, the surface roughness of the post-annealing SBTN thin films increased with an increasing annealing temperature (Fig. 5a). The atomic force microscopy (AFM) images of 0
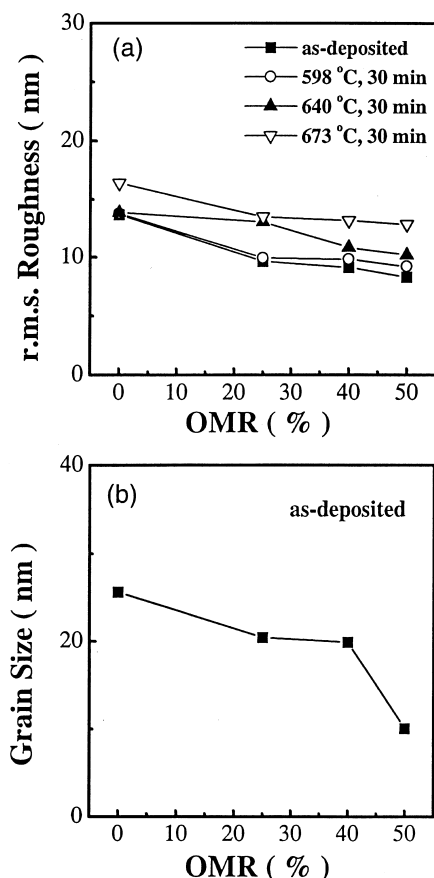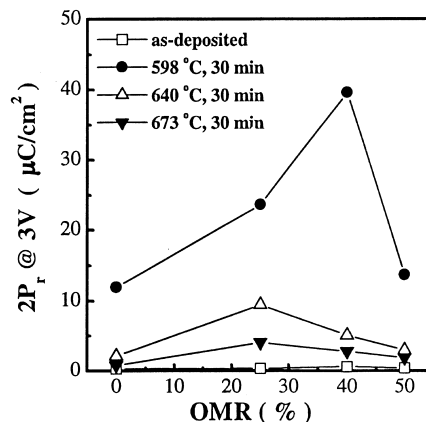

Fig. 6. The dependence of the remanent polarization ($2P_r$) on the OMR and post-annealing temperature.

and 40% OMR films, without and with 673°C post-annealing, indicated that the surface roughness, while decreasing with an increase in OMR, increased with an increase in post-annealing temperature.

Fig. 6 illustrates the dependence of the remanent polarization ($2P_r$) on the OMR with post-annealing. The 40% OMR SBTN film with 598°C post-annealing had a $2P_r$ of 40 $\mu C/cm^2$ at an applied voltage of 3 V. For 598°C post-annealing, the remanent polarization increased with an increasing OMR; however, it attained a maximum value at 40% OMR. According to this figure, further increasing the OMR decreased the remanent polarization. However, the remanent polarization had a maximum value at 25% OMR for 640°C and 673°C post-annealing films. In addition, for the various OMR, 598°C post-annealing films had the largest remanent polarization values.

The SBTN films can exhibit large remanent polarization due to electric dipoles. Previous investigations have indicated that oriented growth [17,20,21], composition [12,13,15,17,22–26], grain size [15], and crystallinity [12] can influence the remanent polarization of the films. Film composition appears to play a profound role in promoting the polarization of electric dipoles, as shown in Fig. 6. XRD data analysis (Fig. 2) reveals that the SBTN films, after a suitable annealing process, exhibited very weak (00*l*) peaks with the *c*-axis oriented normal to the substrate, and a strong (115) reflection. Hence, our films could obtain a large remanent polarization [17,20]. In addition, the 598°C post-annealing could more effectively enhance the crystallinity of SBTN thin films than other post-annealing temperatures (Fig. 2b). Hence, there was maximum remanent polarization in the films with 598°C post-annealing treatment. The Sr ions in SBTN did not have a covalent bonding with the surrounding O ions, which was in contrast to the substituted Bi ions at Sr site [24,25]. Due to the covalent interaction, the Bi ions, rather than the Sr ions, favored displacement, which

Fig. 5. Variation of: (a) r.m.s. surface roughness; and (b) grain size of the films with OMR and post-annealing temperature indicated.

corresponded to the observation that the remanent polarization of Sr-deficient and Bi-excess SBTN was larger than that of stoichiometric SBTN [24,25]. Moreover, the composition of SBTN with an optimum value of Sr(0.8), Bi(2.5), Ta(1.2), and Nb(0.9) could obtain the maximum remanent polarization [12,17,23,25,26]. On the basis of the inductive coupled plasma-atomic emission spectroscopy (ICP-AES) data (Fig. 3), the composition of 40% OMR SBTN was close to this optimum value. Therefore, there was maximum remanent polarization for 40% OMR films without post-annealing and with 598°C post-annealing. However, during 640°C and 673°C post-annealing, the composition of 25% OMR SBTN was close to Bi = 2.5 (Fig. 3). Consequently, the maximum remanent polarization occurred for the 25% OMR films. The film composition appeared to dominate the dielectric and electrical properties of the films. Although the grain size of SBTN films decreased with an increase of the OMR up to 50% (Fig. 5b), the polarization had a maximum value at 40% OMR. Hence, the grain size influenced the properties of the films to a lesser extent than the composition.

Fig. 7 illustrates the polarization vs. electric field curves recorded with −3 to +3 V excitations. The polarization of 40% OMR films with 598°C post annealing had the maximum remanent polarization and $2E_c$ of 77 kV/cm. The remanent polarization and coercive field of the 25% and 40% OMR films with 598°C post-annealing were 23 μC/cm², 40 μC/cm² and 80 kV/cm, 77 kV/cm at an applied voltage of 3 V, respectively (Fig. 8). Moreover, the remanent polarization and coercive field nearly attained saturation at over 3 V. We believe that these results indicated superior properties of SBTN than those in other investigations [8,12,16,17,23,25–27]. These excellent properties, possibly attributed to the unique solid solution of $SrBi_2Ta_2O_9$ and $SrBi_2Nb_2O_9$, made the remanent polarization value of our SBTN films comparable with that of PZT.

Fig. 8. The remanent polarization and coercive field of the 25% and 40% OMR SBTN thin films with 598°C post-annealing as a function of applied voltage.

Fig. 9 depicts the dependence of the dielectric constant and leakage current on the OMR for the films with 598°C post-annealing. The 40% OMR film had a dielectric constant of 752 at an applied voltage of 0 V and a leakage current of 6×10^{-6} A/cm² at an electric field of 50 kV/cm with a time delay of 30 s. Although the dielectric constant and the leakage current increased with an increase in OMR, it reached a maximum value at 40% OMR. According to this figure, further increasing the OMR decreased the dielectric constant and leakage current. The relation of polarization P and dielectric constant ε_r could be obtained analytically using the following equation:

$$P = \varepsilon_o * \int (\varepsilon_r - 1) \mathrm{d}E \qquad (1)$$

where E is an applied field, and ε_o is the dielectric constant in free space. The SBTN films could exhibit a large dielectric constant due to polarization of electric dipoles. Hence, the 40% OMR thin films with 598°C post-annealing had a maximum dielectric constant due to strong (115) and (220) reflections of its XRD pattern (Fig. 2b) and its maximum remanent polarization.

The SBTN films exhibited a leakage current due to dielectric loss. The dielectric loss normally comes from two mechanisms: resistive loss and relaxation loss. In the resistive loss mechanism, mobile charges (electrons and holes) in the film consume the energy. The case of relaxation loss, the mechanism is the relaxation of the dipole, which expends the energy. If the insulating film contains very few mobile charges, the relaxation loss would be the dominant mechanism [28]. According to a previous investigation, the most probable compensation with the substitution of Bi ions at the Sr site in Sr-deficient and Bi-excess SBTN is due to cation vacancies, rather than changes in the cation valency [24]. The difference in valency between the Sr and Bi ions ap-
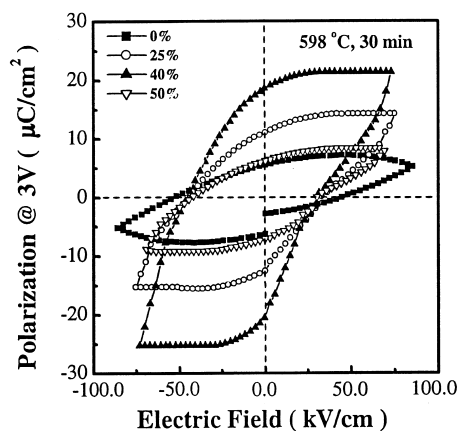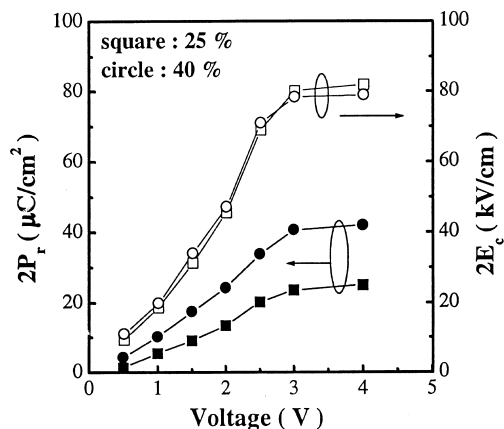
Fig. 7. The polarization vs. electric field curves of various OMR SBTN films with 598°C post-annealing.
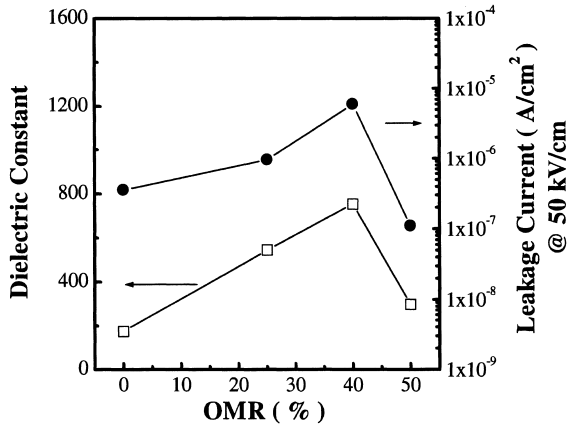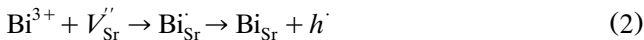
Fig. 9. The dependence of the dielectric constant and leakage current of the 598°C post-annealing films on the OMR.

peared to be attributable to compensation due to the change in the Bi ion valency in the Sr site, i.e.:

$$Bi^{3+} + V''_{Sr} \to Bi^{\cdot}_{Sr} \to Bi_{Sr} + h^{\cdot} \qquad (2)$$

where Bi^{3+}, V''_{Sr}, $Bi^{\cdot}_{Sr}$, Bi_{Sr} and $h^{\cdot}$ represent the excess Bi ions, Sr vacancy, Bi ion on Sr site with charge, Bi ion on Sr site without charge and hole, respectively. According to Eq. (2), the SBTN material tends to show a p-type conductivity. Moreover, the conductivity is usually large, due to the holes produced with 20% Sr-deficient (Sr = 0.8) and 25% Bi-excess (Bi ~ 2.5) in SBTN thin films.

High temperature deposition of SBTN films under non-oxidizing atmosphere, such as Ar, generally produces oxygen vacancies in the film according to:

$$O_o \leftrightarrow V^{\cdot\cdot}_o + 2e' + 1/2O_2 \qquad (3)$$

where O_o, $V^{\cdot\cdot}_o$ and e' represent the oxygen ion on its normal site, oxygen vacancy and electron, respectively. According to Eq. (3), the concentration of the electrons produced with the existence of oxygen vacancies is usually small when the OMR is increased [29–31]. In addition, the concentration of the oxygen vacancies in the perovskite oxide films is much smaller, i.e. approximately 0.0001 M [32]. As expected, the concentration of holes in our high-OMR films was relatively higher than that of the electrons, which was attributed to the holes produced in the films with 20% Sr-deficient and 25% Bi-excess. Fig. 9 indicates that the leakage current density increased with an increase in OMR of up to 40%, which was possible owing to the reduction in concentration of the electrons in the films sputtered at higher OMR to compensate for the holes. According to Fig. 3, the Bi concentration decreased rapidly in the films deposited at above 40% OMR, which may be attributed to a decrease in the concentration of holes which decreased the leakage current density.

According to Fig. 9, the dielectric constant attains a maximum value at 40% OMR with 598°C post-annealing, due to the maximum remanent polarization. In addition, although the leakage current increases with an increasing OMR, it attains a maximum value at 40% OMR, due to the change in ratio of electrons to holes in the SBTN films. Further increasing the OMR decreases the leakage current, due to the decrease of the concentration of Bi in the SBTN films. Hence, the composition effect (Sr-deficient and Bi-excess) dominates the electrical properties of the films sputtered at various OMR.

The loss tangent and resistivity of the films are also a function of OMR, as shown in Fig. 10. The 40% OMR film had a loss tangent of 0.035 at 100 kHz. Both the minimum resistivity and maximum loss tangent occurring at 40% OMR correlated with the results in Fig. 10. In addition, the loss tangent was due to the leakage current loss by a parallel resistance. Moreover, the change in loss tangent was closely associated with the change in the resistivity and leakage current in the various OMR films (Figs. 9 and 10). Therefore, the conduction mechanism in these films would be resistive loss. Restated, the energy was consumed by mobile charges (holes, electrons, and oxygen vacancies) in the film. The variations of loss tangent and resistivity were closely related to the concentration change of mobile charges.

Fig. 11 summarizes the fatigue characteristics of the SBTN films deposited at 25, 40, and 50% OMR with 598°C post-annealing. The fatigue test was performed using a bipolar square wave of 3 V at 1 MHz. These exhibited only slight degradation of polarization at ±3 V square wave after 10^{11} cycles. The results confirmed that the sputtered SBTN films did not experience any fatigue problem, which was commonly observed in PZT films. The measured value of $Q_{sw} = p^* - p^{\wedge}$ was approximately 20 μC/cm^2 for 40% OMR SBTN films with 598°C post annealing. Fig. 12 illustrates that the
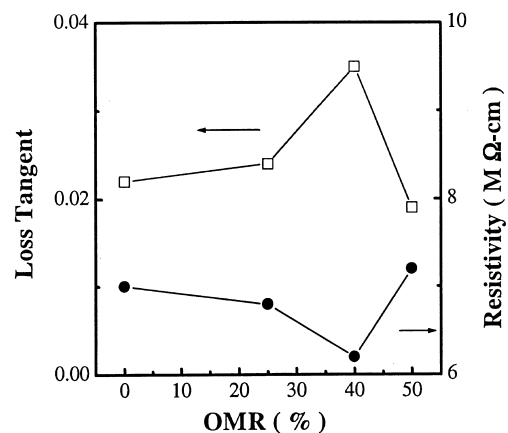

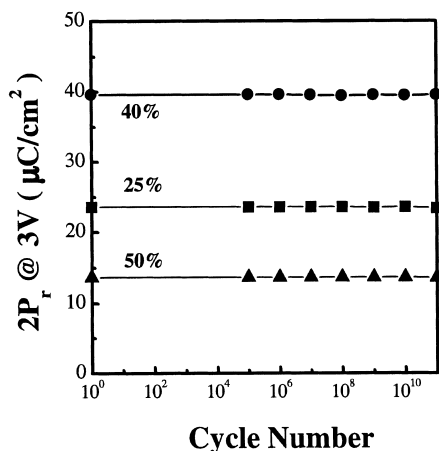Fig. 10. The dependence of the loss tangent and resistivity of the 598°C post-annealing films on the OMR.

Fig. 11. Polarization fatigue of the 25, 40 and 50% OMR SBTN films with 598°C post-annealing.

polarization of 25% and 40% OMR films was degraded by less than 0.5% per decade up to 240 min. A previous investigation revealed that the bulk ionic conductivities of SBTN were much higher than those of the perovskite ferroelectric, e.g. PZT [7]. The high ionic conductivities have allowed us to infer that the good fatigue resistance of SBTN was due to the easy recovery of defects. More specifically, oxygen vacancies entrapped within the capacitors were easily released, resulting in a limited space charge buildup and domain wall pinning during the polarization reversal process [7]. The ionic conductivities of SBTN with various OMR ($\sim 10^{-7}$ S/cm) were much higher and close to the electrical conductivities (Fig. 10).

Fig. 13a,b depict the leakage current, with a time delay of 30 s, of 25% and 50% OMR films with 598°C post annealing, under different 200-s stress fields. The leakage currents of 25% OMR films under 50, 100 and 200 kV/cm stress fields degraded, while those of 50% OMR films under 50 and 100 kV/cm stress fields did not degrade; however, degradation occurred in the
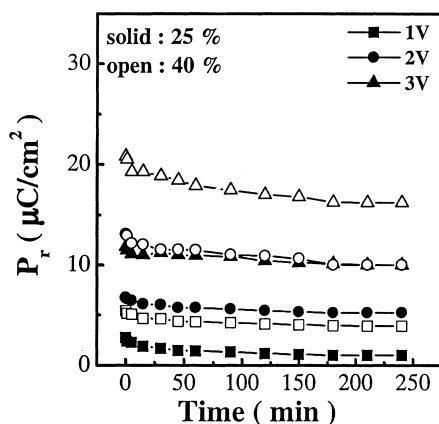

Fig. 12. Polarization of the 25% and 50% OMR SBTN films with 598°C post-annealing, as a function of retention time.
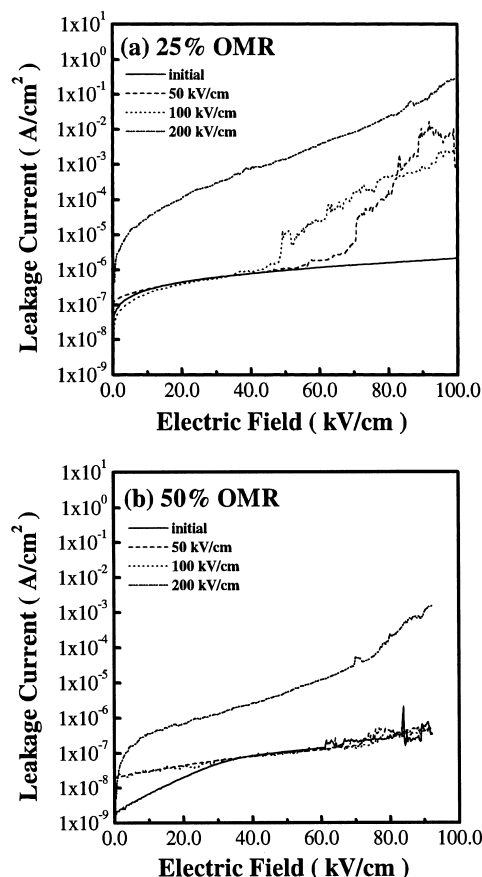

Fig. 13. The leakage current with delay time 30 s of SBTN films deposited at: (a) 25%; and (b) 50% OMR with 598°C post annealing as a function of electric field with 200 s stress.

films after exposure to a 200 kV/cm stress field. The leakage current degradation in 50% OMR films under 200 kV/cm was smaller than in 25% OMR films. Therefore, the dc reliability of SBTN films could be improved by high OMR deposition. The possible mobile charges for SBTN films were holes, electrons, and oxygen vacancies. The holes and electrons were only the transfer carriers and could not accumulate at the interface and grain boundaries. Hence, the entrapped oxygen vacancies degraded the leakage current of the SBTN films. The leakage current under a 'low DC stress field' did not degrade because the migration of oxygen vacancies was depressed by the grain boundary. The leakage current under a 'high DC stress field' degraded because the migration and creation of oxygen vacancies under a high DC stress field occurred. Moreover, the migration of oxygen vacancies towards the cathode and the piling up of oxygen vacancies near the cathode definitely lowered the resistance of the Schottky junction, which would increase the leakage current. However, high OMR deposition can reduce the DC degradation of SBTN films.

Fig. 14a,b depicts the leakage current, with a time delay of 30 s, of 25% and 50% OMR films with 598°C
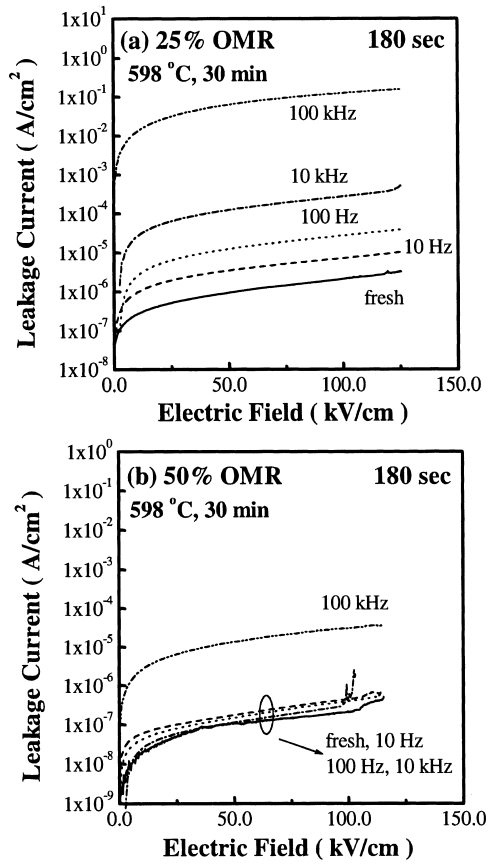
Fig. 14. The leakage current with delay time 30 s of SBTN films deposited at: (a) 25%; and (b) 50% OMR with 598°C post annealing as a function of electric field with a ±10-V square wave ac stress frequency and 180 s stress.

post annealing, under a different ±10 V square wave 180-s ac stress frequency. The leakage currents of 25% OMR films under 10, 100, 10 k and 100 kHz stress frequencies degraded, while those of 50% OMR films under 10, 100 and 10 kHz stress frequencies did not degrade; however, degradation occurred in the film after a 100-kHz stress frequency. Under the 100-kHz stress frequency, the leakage current degradation in the 50% OMR films was much smaller than in the 25% OMR films. Therefore, the ac reliability of SBTN films could also be improved by high OMR deposition. The oxygen vacancy was referred to as an electron trapping state, where the predominant charge exchange was between the conduction band and the trap level. Under ac stress applied at Schottky junction, the depletion layer width varied about its equilibrium position due to trapping and detrapping of electrons from the oxygen vacancies [33]. The ac degradation of SBTN films could be improved by higher OMR with less oxygen vacancies.

Lifetime extrapolation using constant voltage stress–time dependent dielectric breakdown (TDDB) studies (Fig. 15) predicted the 10-year lifetime at a 1-V operat-

ing voltage. Fig. 15 indicated that the characteristic time (t_{ch}) depended on the electric field. The characteristic time (t_{ch}) was defined as the time when the current density shows a value larger than the minimum by one order ($\times 10$) under DC stress. The characteristic time (t_{ch}) increased with a decrease of the electric field. This finding suggested that the 50% OMR film has a longer lifetime than the 0, 25, and 40 OMR films. The TDDB, as shown in Fig. 15, was also referred to as the resistance degradation of dielectrics, which showed a slow increase of leakage current under DC field stress. Hence, the SBTN films degraded owing to the deterioration of Schottky interface barrier.

Available theories attempting to account for the degradation mechanism of perovskite titanates can be categorized as either grain boundary model or reduction model [34]. In the grain boundary model, a DC field-induced deterioration of the grain boundaries is responsible for the degradation phenomenon. In the reduction model, the positively charged oxygen vacancies with a relative high mobility electromigrate towards the cathode under DC electric field. The oxygen vacancies then pile up at the front of cathode and are compensated for by the electron injected from cathode. The outcome is that the space charge accumulation at grain boundaries and interface of SBTN and metal reduces the grain boundary height and interface barrier height and, then, increases the leakage current. Results in this study are related to the grain boundary and reduction models, as follows: (1) the 50% OMR SBTN has more 'grain boundaries' than lower OMR SBTN because the grain size of 50% OMR SBTN is smaller (Fig. 5b). Therefore, as expected, the 50% OMR SBTN has a longer lifetime on the basis of the grain boundary model, which was verified by the results in Fig. 15; and (2) the 50% OMR SBTN contains a low concentration of oxygen vacancies compared to 25% OMR film. Hence, the 50% OMR SBTN film has a smaller degradation and longer lifetime. On the basis
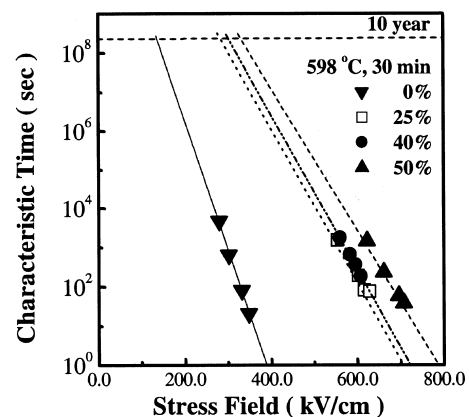

Fig. 15. Time to breakdown of the various OMR SBTN films with 598°C post-annealing as a function of stress field.

of three separate complex planes (capacitance, impedance and admittance) analyses, the defect densities of 25% and 50% OMR films were 5.5×10^{16} and 1.7×10^{16} cm^{-3}, respectively. The 50% OMR SBTN had less defects than the 25% OMR sample. According to the prediction of reduction model, the deterioration of 50% OMR SBTN was smaller. In fact, the TDDB was significantly improved in the high OMR sample as compared to low OMR sample (Fig. 15).

4. Conclusions

This work investigated the effect of the annealing process on the ferroelectric properties of various OMR sputtered SBTN thin films. Experimental results indicated that annealing can effectively obtain a large remanent polarization. The remanent polarization, dielectric constant and leakage current of 598°C post-annealing SBTN thin films increased with an increase in the OMR and reached a maximum value at 40% OMR. Results obtained from the dielectric constant and the leakage current were interpreted on the basis of polarization effect and loss theory. The 400-nm thick 40% OMR SBTN films with 598°C post-annealing exhibited good surface morphology and had a dielectric constant of 752, a loss tangent of 0.035 at 100 kHz, a leakage current density of 6×10^{-6} A/cm^2 at an electric field of 50 kV/cm with a delay time of 30 s, remanent polarization ($2P_r$) of 40 μC/cm^2 and coercive field ($2E_c$) of 77 kV/cm at an applied voltage of 3 V. The 10-year lifetime of the time-dependent dielectric breakdown studies indicated that high OMR samples have longer lifetime than the other lower OMR samples. The SBTN films demonstrated fatigue free characteristics up to 10^{11} switching cycles under a 3-V bipolar 1 MHz square wave. Moreover, the polarization of the films degraded less than 0.5% per decade up to 240 min.

Acknowledgements

References

[1] J. Kudo, Y. Ito, S. Mitarai, N. Ogata, S. Yamazaki, H. Urashima, A. Okutoh, M. Nagata, K. Ishihara, Int. Electron. Devices Meet. Tech. Dig. 34 (1997).

[2] M. Takeo, M. Azuma, H. Hirano, K. Asari, N. Moriwaki, T. Otsuki, K. Tatsuuma, Int. Electron. Devices Meet. Tech. Dig. 38 (1997).

[3] R. Dat, H.D. Shih, in: R.K. Pandey, D.E. Witter, U. Varshneg (Eds.), 99th Annual Meeting of the American Ceramic Society Cincinnati, Ohio, U.S.A., May 4–7, 1997, Proceedings of the Symposium on Integrated Thin Films and Applications, , 1997, p. 1.

[4] M. Suzuki, J. Ceram, Soc. Jpn. 103 (1995) 1088.

[5] T. Mihara, H. Yoshimori, H. Watanabe, C.A.P.D. Araujo, Jpn. J. Appl. Phys. 34 (1995) 5233.

[6] D. Dimos, H.N.A. Shareef, W.L. Warren, B.A. Tuttle, J. Appl. Phys. 83 (1996) 1682.

[7] T.C. Chen, C.L. Thio, S.B. Desu, J. Mater. Res. 12 (1997) 2628.

[8] R. Dat, J.K. Lee, O. Auciello, A.I. Kingon, Appl. Phys. Lett. 67 (1995) 572.

[9] T. Kanehara, I. Koiwa, Y. Okada, K. Ashikaga, H. Katoh, K. Kaifu, Int. Electron. Devices Meet. Tech. Dig. 42 (1997).

[10] S.I. Ohfuji, M. Itsumi, Jpn. J. Appl. Phys. 37 (1998) 2559.

[11] D.J. Taylor, R.E. Jones, Y.T. Lii, P. Zurcher, P.Y. Chu, S.J. Gillespie in: S.B. Desu, R. Ramesh, B.A. Tuttle, R.E. Jones, I.K. Yoo (Eds.), Ferroelectric Thin Films V, Pittsburgh, PA, U.S.A., 1996, Mat. Res. Soc. Symp. Proc. 433 (1996) 97.

[12] I. Koiwa, K. Tani, J. Mita, T. Iwabuchi, Jpn. J. Appl. Phys. 37 (1998) 192.

[13] T. Osaka, A. Sakakibara, T. Seki, S. Ono, I. Koiwa, A. Hashimoto, Jpn. J. Appl. Phys. 37 (1998) 597.

[14] S.B. Desu, P.C. Joshi, S.O. Ryu, Appl. Phys. Lett. 71 (1997) 1041.

[15] J. Zhu, X. Zhang, Y. Zhu, S.B. Desu, J. Appl. Phys. 83 (1998) 1610.

[16] K. Miura, M. Tanaka, Jpn. J. Appl. Phys. 37 (1998) 606.

[17] H.M. Tsai, P. Lin, T.Y. Tseng, Appl. Phys. Letts. 72 (1998) 1787.

[18] T. Horikawa, N. Mikami, T. Makita, J. Tanimura, M. Kataoka, K. Sato, M. Nunoshita, Jpn. J. Appl. Phys. 32 (1993) 4126.

[19] M.S. Tsai, S.C. Sun, T.Y. Tseng, IEEE Trans. Electron. Devices 46 (1999) 1829.

[20] S.B. Desu, D.P. Vijay, X. Zhang, B. He, Appl. Phys. Lett. 69 (1996) 1719.

[21] I. Koiwa, T. Kanehara, J. Mita, T. Iwabuchi, T. Osaka, S. Ono, Jpn. J. Appl. Phys. 36 (1997) 1597.

[22] H. Watanabe, T. Mihara, H. Yoshimori, C.A.P.D. Araujo, Jpn. J. Appl. Phys. 34 (1995) 5240.

[23] T.C. Chen, T. Li, X. Zhang, S.B. Desu, J. Mater. Res. 12 (1997) 2165.

[24] K. Miura, M. Tanaka, Jpn. J. Appl. Phys. 37 (1998) 2554.

[25] T. Noguchi, T. Hase, Y. Miyasaka, Jpn. J. Appl. Phys. 35 (1996) 4900.

[26] H.M. Tsai, P. Lin, T.Y. Tseng, J. Appl. Phys. 85 (1999) 1095.

[27] Y.T. Kim, D.S. Shin, Appl. Phys. Lett. 71 (1997) 3507.

[28] P. Li, J.F. Mcdonald, T.M. Lu, J. Appl. Phys. 71 (1992) 5596.

[29] C.S. Hwang, S.O. Park, H.J. Cho, C.S. Kang, H.K. Kang, S.I. Lee, M.Y. Lee, Appl. Phys. Lett. 67 (1995) 2819.

[30] R.M. Waser, J. Am. Ceram. Soc. 72 (1989) 2234.

[31] D.M. Smyth, M.P. Harmer, P. Peng, J. Am. Ceram. Soc. 72 (1989) 2276.

[32] M.S. Tsai, T.Y. Tseng, Mater. Chem. Phys. 57 (1998) 47.

[33] Y. Fukuda, K. Numata, K. Aoki, A. Nishimura, Jpn. J. Appl. Phys. 35 (1996) 5178.

[34] R. Waser, T. Baiatu, K.H. Hardtl, J. Am. Ceram. Soc. 73 (1990) 1645.